Microseismic Study of Menengai Caldera: Geothermal Prospect in the Central Kenya Dome

[1]Ezer Patlan, [2]Antony Wamalwa, [1]Galen Kaip, [1]Ashley Grijalva, and [1]Aaron A. Velasco

[1]University of Texas at El Paso, 500 West University Ave., El Paso, TX 79968
[2]Geothermal Development Company, Taj Tower, 9th Floor, Upper hill, P.O. Box 100746, 00101, Nairobi, Kenya

epatlan@miners.utep.edu

Keywords: Earthquakes, Ambient Noise Cross-correlation, SKS shear-wave splitting, and Hydrothermal

ABSTRACT

The Geothermal Development Company (GDC) and the University of Texas at El Paso (UTEP) have deployed fourteen seismic stations around the Menengai geothermal field along the Kenya rift system to monitor the seismicity around the host volcano in order to identify active faults and fracture systems that may contain hydrothermal fluids and favorable drilling targets. Double difference relocation is being used to locate events and image faults at the margin of the caldera. We also use teleseismic events (50 thus far) with a minimum magnitude (M_w) of 5.4 to calculate SKS shear wave splitting so as to approximate the fast direction and splitting delay time. Finally, we are applying ambient noise tomography to identify the hydrothermal reservoir zone.

1. INTRODUCTION

Geophysical studies over geothermal fields can provide fundamental information about the subsurface structures and processes that are key to sitting high producing wells to tap the resource (e.g., Simiyu and Keller, 2000; Simiyu, 2000, 2009; Wilson et al., 2003). Although resistivity and potential field (gravity and magnetic) methods have been used to identify faults and fractures and intrusions (e.g. Árnason et al., 2010; Newman et al., 2008; Wamalwa et al., 2011), the techniques can also be used to identify the depth range of active faults that can led to fluid channels of an inactive fault. Micro-earthquake studies can help in identifying active faults from accurate event locations, and could thus be used to infer fluid movement. In addition, microseismic relocation can facilitate in locating the brittle-ductile transition zone in order to identify porosity changes. With this information, we can provide information on where to target drilling of the geothermal reservoir. Hence, the main goal of this project is to collect and analyze seismic data with a view to identifing the fluid pathways and zones with fluid phase change.

In order to accomplish these goals, the Geothermal Development Company (GDC) and the Department of Geological Sciences at the University of Texas at El Paso (UTEP) installed a total of fourteen seismometers around the Menengai. Seven instruments (Phase 1) were installed in March 2011 and the other seven (Phase 2) in August, 2011. Here, we present the initial results of first five months of recording from Phase 1.

1.1 Menengai Geology and Previous Geophysical Studies

The Menengai volcano is located at the intra-continental crustal triple junction north of the Nakuru-Naivasha basin where the Nyanza rift joins the Kenya rift (Figure 1). The Menengai region is dominated by a central volcano with a large caldera of about 12km in diameter.

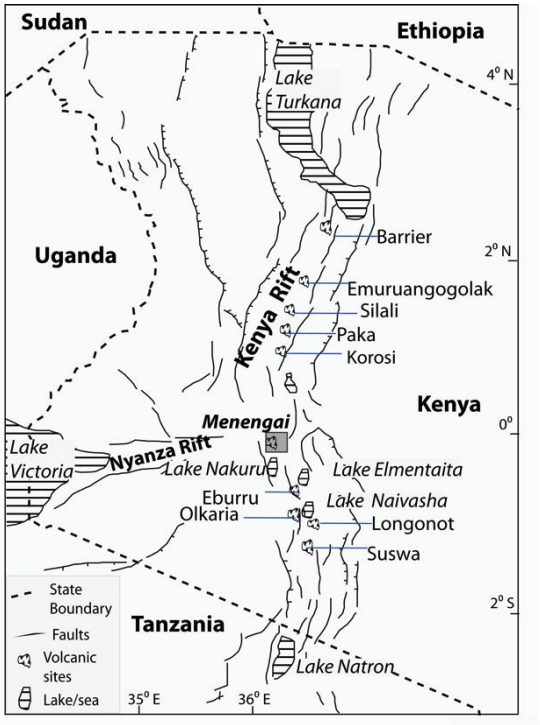

Figure 21: Map of Kenya rift showing the Menengai Caldera along with various volcanoes in the region.

The caldera has steep sides of up to 300m high where old shield lavas are exposed. Pyroclastics and tuffs cover the rest of the area outside the caldera. The volcanic suite comprises of phonolites, trachyphonolites and trachytes. The source of the pyroclastics evolved from the subsequent eruptions that led to the formation of the large caldera.

Previous seismic studies have imaged a high velocity body beneath the Menengai volcano (Simiyu and Keller, 2000). An integrated study that combined seismic and gravity data for the southern section of the rift (Simiyu and Keller, 2001) relocated swarms of micro-events ranging from 0 to 8km depth and showed a distribution of high heat based on the seismicity changes with depth in Olkaria, Kenya. Recent resistivity studies (Wamalwa et al., 2011, in review) have imaged a conductive zone at about 6km deep below the surface, which has been interpreted as molten rocks.

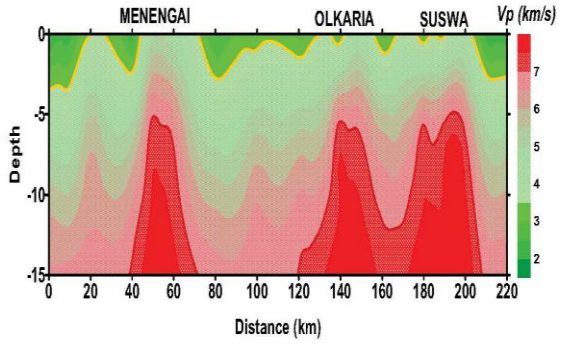

Figure 22: Seismic velocity models along the rift axis showing high Velocity zones beneath Menengai Olkaria and Suswa Volcanic centers (Simiyu and Keller, 2000).

A similar interpretation from micro-earthquake analysis (Simiyu, 2009) observed that most of the events within the caldera were restricted to the upper 6km depth indicating a brittle-ductile transition zones at this depth that suggest the presence of a hot magma material. Our study is aimed at further analyzing micro-earthquakes in this region by locating events precisely, using a double difference approach (HypoDD) and identifying high temperature fluid filled zones that will be favorable for production wells with high yield.

2. DATA AND PROCESSING

Phase 1 of the seismic station deployment comprised of seven stations (Table 1). Our priority for selecting these sites was to adequately cover the Caldera area, and place sites in secure locations. The data presented here was recorded from this station between March and July 2011. A suite of instruments, including broadband, intermediate and short period sensors were deployed to assist in locating earthquakes. In addition to this, a suite of techniques were applied to identify source processes of volcanic earthquakes, including long period events that can potentially identify fluid movement.

Table 1: Site locations for Phase 1 & 2

Station Code	Lat. (°)	Lon. (°)	Elevation (m)	Sensor	Description
			Phase 1		
MNC1	-0.19375	36.08299	1867	HS10	Caldera
BHT	-0.14252	36.15708	2119	3T	School House
LWHS	-0.2222	36.1767	2068	3T	School
RGO	-0.15607	36.04936	1948	40T	School
TOR1	-0.17776	36.00686	1942	HS10	Homestead
KIMU	-0.26657	36.02494	1941	3T	School
VWP	-0.25946	36.09253	2106	40T	Homestead
			Phase 2		
NGSS	-0.1822	36.2446	2730	40T	School
DIGR	-0.0964	35.9846	1700	3T	Homestead
SLS	-0.0999	36.1278	1869	40T	School
NDG	-0.1064	36.0594	2068	40T	School
MNP	-0.2179	35.9466	1991	3T	School
BLS	-0.1145	36.1599	2173	40T	School

Quality checks were conducted on the recorded data continuously by reviewing all data logs, checking for time gaps and timing error. Although excellent recovery rates for the data was noted, there were 1 s time jumps on three stations that were corrected.

3. METHODOLOGY

3.1 Double Difference Earthquake Relocation

After archiving, checking for quality and using the BRTT Antelope Software, we performed automatic detections using a short-term and long-term average (STA/LTA) detection algorithm to identify possible seismic arrivals. We used different filters and detection parameters to search for local events using:

a) A high pass filter at 5 Hz to highlight local impulsive earthquakes (STA of 1 s; LTA of 10 s);
b) A high pass filter at 5 Hz to highlight local emergent (tremor) events (STA of 60 s; LTA of 600 s); and
c) A low pass filter at 20 s to highlight possible long-period events (STA of 60 s; LTA of 600 s).

After the automatic detections were made, we associated arrivals to possible hypothetical events, and developed an automated catalog of earthquakes. The catalog included local events, which were review manually. During review, we re-picked *P* waves and relocated the events using a standard approach to develop a new, local catalog that served as the foundation for our double difference approach.

In order to relocate earthquakes, the seismic network must surround the seismic sources. To determine if an earthquake lied within the network of stations (and could be located with high confidence), we calculated the maximum station-event azimuth, called azimuthal gap, using our catalog. The azimuthal gap is defined as the maximum angle between event-station pairs; and for an event to be within our networks, the azimuthal gap must be less than 180°. To accomplish high precision earthquake locations, we applied the double difference earthquake location method (Waldhauser and Ellsworth, 2000) at Menengai, Caldera. The double difference earthquake location method (hypoDD) uses two important attributes that make earthquake locations high precision: high precision *P* wave arrival times and event clusters to remove dependence on the velocity structure. We manually picked the *P* arrival time for every event previously determined and then compute a cross-correlated time pick for all events and stations.

3.2 SKS Shear Wave Splitting

The teleseismic SKS shear-wave splitting technique can assist in determining present or past mantle deformation processes in rifts, hotspots, oceanic islands, orogens, and continental environments (Wüstefeld et al., 2009). The technique can be used to measure anisotropy beneath a seismic station with good lateral resolution of few tens of kilometers, but has poor vertical resolution. In this study, we determined SKS-splitting measurements using transverse and radial components. We used teleseismic events (epicentral distance range 90˚-130˚) with magnitude (M_w) greater than 5.4. We applied band-pass filters from 0.01 Hz – 0.5 Hz to ensure that there was no frequency-

dependence in the splitting parameters (Ayele et al., 2004) and approximated the shear wave splitting for every seismic station. The shear wave splitting SKS approach (Silver & Chan, 1991) can be used to estimate the time separation between the fast and slow shear waves ¶t and the polarization angle of the fast shear wave f based on grid search. We found the two splitting parameters ¶t and f that best linearizes the particle motion instead of minimizing the energy on the transverse component (Ayele et al., 2004; Wüstefeld et al., 2009).

3.3 Ambient Noise Tomography

We applied an ambient noise tomography technique that had been previously developed (Bensen et al., 2007, 2008 and Lin et al., 2008). We removed the instrumentation response from the Guralp 40T, Guralp 3T, and HS10 sensors, using band-pass filters appropriate for each station pair. We removed the earthquake signals by applying a one-bit normalization, which generated a data stream composed only of the values 1 and -1, retaining only the sign and disregarding the amplitude of the signal completely (Bensen et al., 2007). Spectral whitening was then performed to reduce the seismic amplitude and/or to flatten the spectral over the entire period band (Bensen et al., 2007; Yang et al., 2011; Yang, Shen, and Ritzwoller, 2011). We retrieved the Green's function by cross-correlating the normalized waveforms between two seismic stations in five hour increments, and stacking in 3-month bins to account for seasonal variability and estimate the group velocity uncertainties (Campillo and Paul 2003; Nicolson et al., 2012).

Frequency time analysis done by Herrmann and Ammon (2004) was used to measure the dispersion curves of the Rayleigh waves. The group velocity is the velocity at which the energy-packet travels while the phase velocity describes the velocity of a phase at a given frequency. Both velocities are sensitive to the structure of the rocks through which the surface waves travel.

4. PRELIMINARY RESULTS

4.1 Double Difference Earthquake Relocation

For the initial, automated locations, we used the Antelope software package that automatically and routinely detected the *P* arrival time (Figure 3). We manually re-picked the *P*-wave and relocated the hypocenter using Antelope and HypoDD. Figure 3 shows the initial grid locations from March 2011 to March 2012, which then must be relocated to obtain the preliminary locations that to be used for the double difference approach.

Table 2 shows the parameters that were used to link similar *P*-phase travel time events (using ph2dt) and produce a travel time catalog of event pairs. In order to evaluate the location of the events, a 1-D velocity model from Simuyi and Keller, 2000 was applied in the inversion as initial model. Figure 4 shows our preliminary double difference locations. Note the algorithm has removed a majority of our events, and we will explore the results further to guarantee that we contain the most events possible.

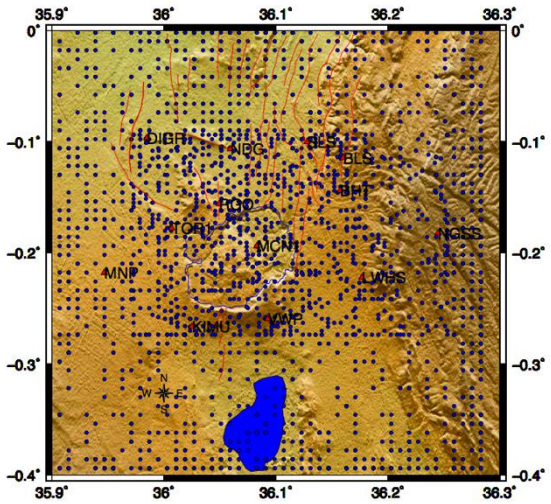

Figure 23: Shows 14 seismic stations (red triangles) deploy in Menengai Caldera. From March 2011 to March 2012, the preliminary local events (blue circles) are grid locations as part of the association algorithm that must be manually re-picked the *P* waves and relocated using Antelope.

Once we had determined a location, we approximated the local magnitude (M_L) using the distance between the station and event (□) and the maximum amplitude (A) of the event:

$$M_L = \log_{10}(A) + 2.76\log_{10}(\Delta) - 2.48 \qquad (1).$$

We removed the instrumentation response and applied a Wood Anderson instrument filter to the seismograph; the local magnitude can be approximated using equation 1.

To determine the characteristics of the brittle-ductile transition zone, we propose the Power Spectral Density (PDS) approach that can be used along with size of the event (local magnitude) to identify a volcanic tectonic, long-period, hybrid, or tremor that can help in classifying a hot springs, fumaroles and hydrothermal system (Chouet, 1996).

Table 2: Parameters used to generate network of delay time links from phase pick data (see Waldhauser, 2001 for parameter description).

MIN WGHT	MAX DIST	MAXSEP	MAX NGH	MIN LNK	MIN OBS	MAX OBS
0.001	60	10	10	4	4	100

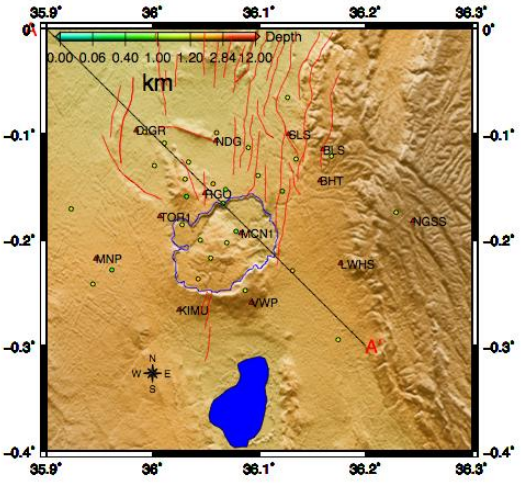

Figure 4: Shows 14 seismic stations (red triangles) deploy in Menengai Caldera. The preliminary local events (color circles) are located north and east-west providence of Menengai caldera.

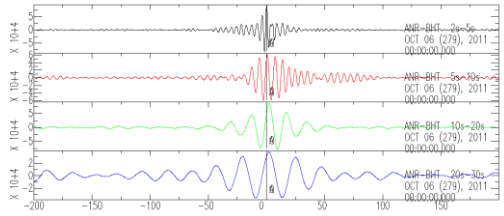

Figure 5: Shows the ambient noise cross correlation between ANR and BHT seismic station with four different band pass filter range from 2s-5s, 5s-10s, 10s-20s, and 20s-30s.

4.2 SKS Shear Wave Splitting

We analyzed the SKS shear wave splitting by using teleseismic events to study deeper earth structure. We will analyze the *P* and *S* shear wave splitting until we have good seismic coverage in the Menengai Network. Wüstefeld et al. (2009) describe that the observed fast direction parallel to plane motion is caused by relative motion between plates and deeper interior of the Earth. Figure 6 shows the azimuth of the fast split shear wave polarization plane that is related to the orientation of the rift system and also illustrates teleseismic SKS shear wave splitting.

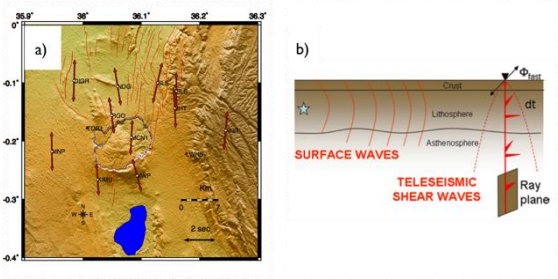

Figure 6: (a) shows the splitting parameters *dt* and *f* that follow the mantle flow direction of the rift system. (b) cartoon illustrating the path and spatial resolution related to the teleseismic SKS shear wave and surface waves.

4.3 Ambient Noise Tomography

We retrieved the Green's Function in Figure 5 by preprocessing the noise using normalization and spectral whiten in order to approximate the group velocity using Frequency time analysis by Herrmann and Ammon (2004). Figure 5 shows the stacked cross-correlation of ANR and BHT seismic station. We filtered four band-pass filters at ANR and BHT ranging from 2s – 30s to analyze the Green's function since each station had a difference sensor. For this application, the 40T sensor (ANR) had a frequency range from 2s – 30s while the 3T sensor (BHT) had a frequency range from 2s – 110s. After analyzing the ambient noise cross-correlation, we applied a multiple frequency analysis to approximate the group velocities.

Figure 5 shows Rayleigh-wave Green's function between stations ANR and BHT filtered in different frequency bands and stacked for six months. We will approximate the group velocity using FTAN and MTA, and we are processing the total of 78 possible station cross-correlation pairs. The group velocity will be input into a tomography analysis.

5. CONCLUSION

Our preliminary local earthquake locations (Figure 3) appear to be scattered within the caldera, but by acquiring more data for the next two years, we believe our analysis can approximate the hydrothermal system that could target potential drilling sites. In the future, we will process our data for source characterization (i.e., tremor, swarm identification, etc.), and crustal structure determination (receiver functions, tomography, etc.).

REFERENCES

Árnason, K., and Eysteinsson, H.: Join 1D inversion of TEM and MT data and 3D inversion of MT data in the Hengill area, SW Iceland, *Geothermics*, **39**, (2010), 13-34.

Ayele, A., Stuart, G., and Kendall, J.M.: Insights into rifting from shear wave splitting and receiver functions: an example from Ethiopia, *Geophysical Journal International*, **157**, (2004), 354-362.

Bensen, G.D., Ritzwoller, M.H., Barmin, M.P., Levshin, A.L., and Lin, F.: Processing seismic ambient noise data to obtain reliable broad-band surface wave dispersion measurements, *Geophysical Journal International*, **169**, (2007), 1239-1260.

Bensen, G.D., Ritzwoller, M.H., and Shapiro, N.M.: Broadband ambient noise surface wave tomography across the United States, *Journal of Geophysical Research*, **113**, (2008), 1-21.

Campillo, M., and Paul, A.: Long-range correlations in the diffuse seismic coda, *Science*, **299**, (2003), 547-549.

Chouet, B.A.: Long-period volcano seismicity: Its source and use in eruption forecasting, *Nature*, **380**, (1996a).

Hermann, R.B., and Ammon, C.J.: surf96 from computers programs in seismology, surface waves, receiver functions and crustal structure, version 3.30, Department of Earth and Atmospheric Sciences, Saint Louis University, (2004).

Kennet, B.L.N.: Seismic Wave Propagation in Stratified Media, *Cambridge University Press*, Cambridge, England, (1983), 1-342.

Langston, C.A.: A body wave inversion of the Koyna, India earthquake of December 10, 1967, and some

implications for body wave focal mechanisms, *Journal of Geophysical Research*, **81**, (1976), 2517-2529.

Langston, C.A.: Source inversion of seismic waveforms: The Koyna, India, earthquakes of 13 September, 1967, *Bulletin of the Seismological Society of America*, **71**, (1981), 1-24.

Lin, F.C., Moschetti, M.P., and Ritzwoller, M.H.: Surface wave tomography of the western United States from ambient seismic noise: Rayleigh and Love wave phase velocity maps, *Geophysical Journal International*, **173**, (2008), 281-298.

Nicolson, H., Curtis, A., Baptie, B., and Galetti, E.: Seismic interferometry and ambient noise tomography in the British Isles, *Proceeding of the Geologist's Association*, **123**, (2012), 74-86.

Randall, G.E., Ammon, C.J., and Owens, T.J.: Moment tensor estimation using regional seismograms from a Tibetan Plateau portable network deployment, *Geophysical Research Letters*, **22**, (1995), 1665-1668.

Ritsema, J., and Lay, T.: Rapid source mechanism determination of large (Mw $\geq$ 5) earthquakes in the western United States, *Geophysical Research Letters*, **20**, (1993), 1611-1614.

Silver, P.G., and Chan, W.W.: Shear wave splitting and subcontinental mantle deformation, *Journal Geophysical Research*, **96 B(10)**, (1991), 16429-16454.

Simiyu, S.M., and Keller, G.R.: Geophysical interpretation of the upper crustal structure of the southern Kenya rift, *Geophysical Journal International*, **1245**, (2001), 234-267.

Simiyu, S.M.: A volcano-seismic approach to geothermal exploration, 5th World Geothermal Congress 2000, Morioka, Japan, (2000).

Simiyu, S.M.: Application of micro-seismic methods to geothermal exploration: examples from the Keyna rift, *United Nations University and LaGeo*, **1**, (2009), 1-27.

Waldhauser, F.: HYPODD—A program to compute double-difference hypocenter locations, *U.S. Geological Survey Open-File Report*, (2001).

Waldhauser, F., and Ellsworth, W.L.: A Double-Difference Earthquake Location Algorithm: Method and Application to the Northern Hayward Fault, California, *Bulletin of the Seismological Society of America*, **90**, (2000).

Wilson, D., Aster, R., and RISTRA Team: Imaging crust and upper mantle seismic structure in the southwestern United States using teleseismic receiver functions, *Leading Edge*, **22**, (2003), 232-237.

Wüstefeld, A., Bikelmann, G., Barruol, G., and Montagner, J.P.: Identifying global seismic anisotropy patterns by correlating shear-wave splitting and surface-wave data, *Physics of the Earth and Planetary Interiors*, **176**, (2009), 198-212.

Yang, Y., Ritzwoller, M.H., and Jones, C.H.: Crustal structure determined from ambient noise tomography near the magmatic centers of the Coso region, southeastern California, *Geochemistry Geophysics Geosystems*, **12**, (2011), 1-20.

Yang, Y., Shen, W., and Ritzwoller, M.H.: Surface wave tomography on a large-scale seismic array combining ambient noise and teleseismic earthquake data, *Earthquake Sciences*, **24**, (2011), 55-64.